Liquid Crystals ISSN 0267-8292 print/ISSN 1366-5855 online # 2003 Taylor & Francis Ltd
http://www.tandf.co.uk/journals
DOI: 10.1080/02678290310001621886

we study the structural features of nucleation and the initial growth of TFCDs caused by the electric field in a homeotropic cell with a SmA material that is doped with nanoparticles.

Li and Lavrentovich [2] investigated the scenario of the electric field-induced transition in a geometry similar to the present study, but for an undoped SmA material. They demonstrated that the transition is a two-step process. During the first step, as the voltage gradually increases, TFCDs of micron or submicron size a^* nucleate at different sites in the cell. These sites have either bulk or surface imperfections. Upon further field increase, the radius a of the TFCD increases, but only to some critical radius a^{**}, of the order of the cell thickness h. At $a > a^{**}$, the TFCD changes into a stripe domain (SD); the object looses its circular symmetry. Thus a field-induced stable TFCD in the restricted geometry of a homeotropic cell has two characteristic sizes: the minimum a^* size below which a TFCD embryo is unstable with respect to the unperturbed configuration of flat smectic layers, and a maximum size a^{**} above which the TFCD is unstable with respect to a SD. The two steps in the TFCD growth are controlled by different contributions to the free energy of the system [2, 3]. The first step, when $a^* < a < a^{**}$, is controlled mainly by (a) dielectric coupling energy of the anisotropic SmA phase and the electric field, (b) elastic energy of deformations in the TFCDs, and (c) energy of distortions around imperfections in the bulk of the material or at the surfaces of the cell. During the second step, $a > a^{**}$, the surface anchoring of the smectic layers at the bounding plates of the cell begins to play an increasingly significant role since TFCDs of large size inevitably require large deviations of layers from their initial orientations at the boundaries (parallel to the confining walls of the cell); non-zero surface anchoring leads to the morphological TFCD–SD change [2].

Nanoparticles in the liquid crystal might serve as nucleation sites along with other irregularities, such as spacers and the air–liquid crystal interface at the edge of the cell. The goal of this project is to investigate the initial growth of the TFCD until it reaches the critical diameter a^{**} before the transition to the striped phase takes place, and also to monitor the growth of SD at scales larger than a

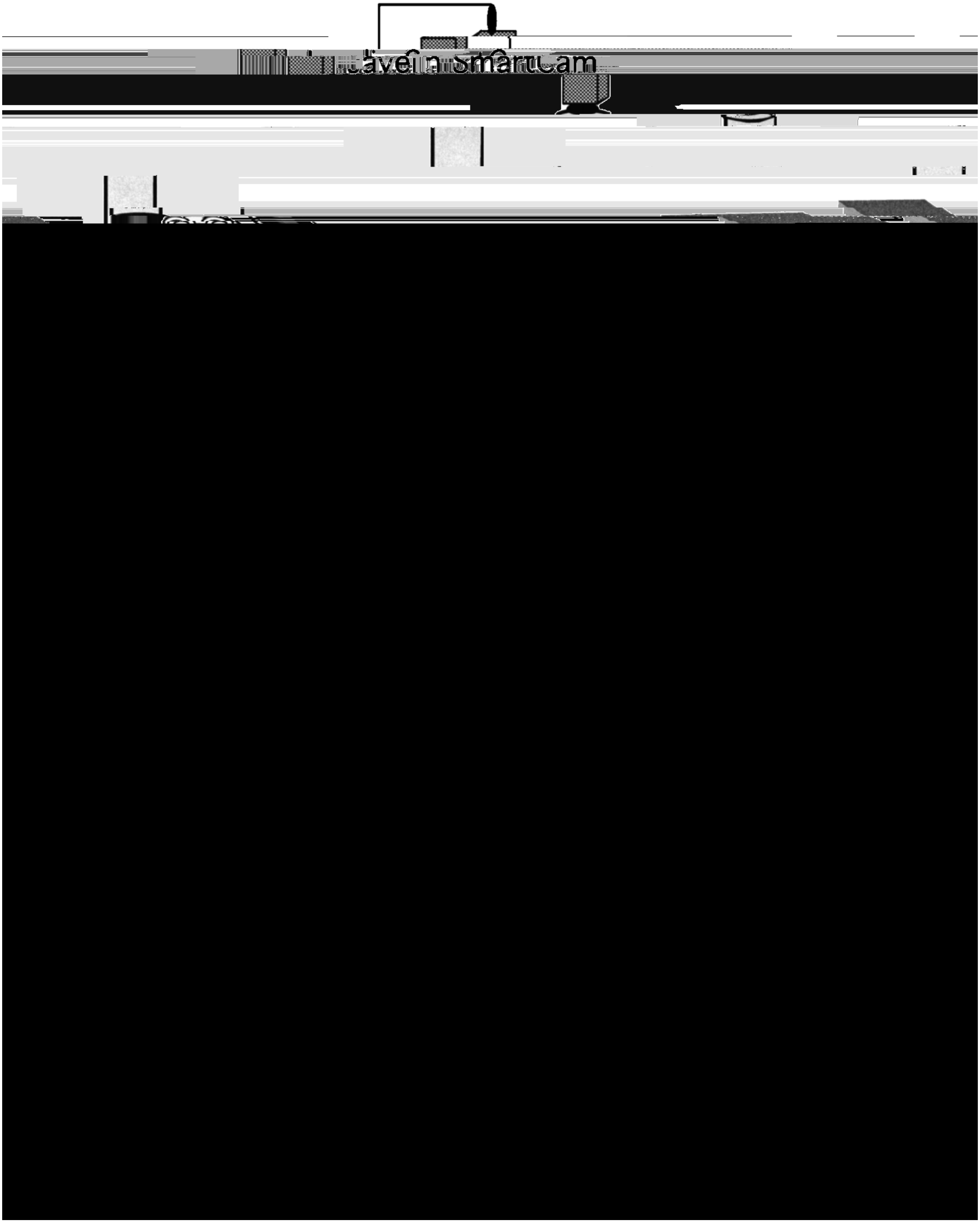
Javelin SmartCam

Figure 1. Experimental set-up.

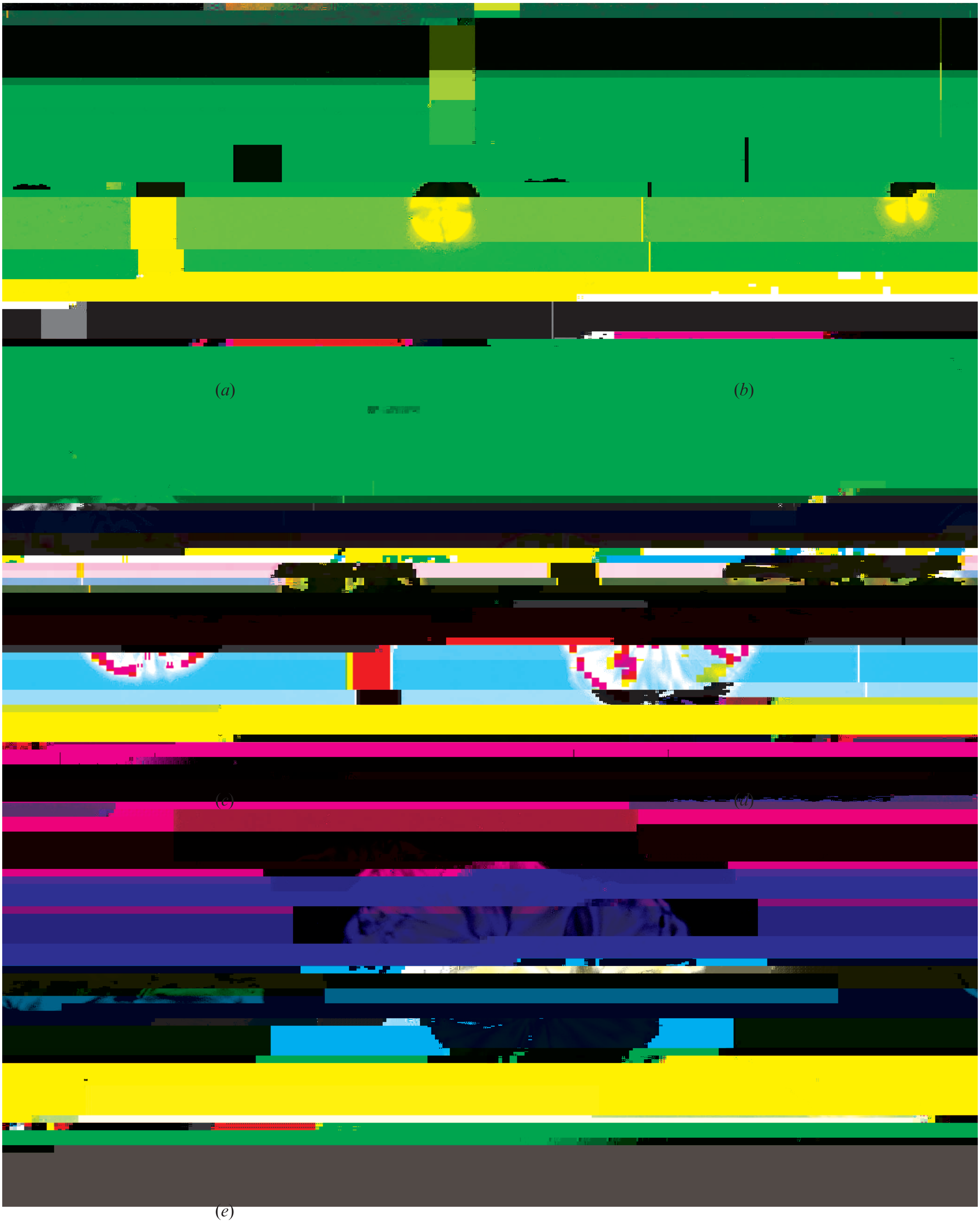

Figure 2. Nucleation and growth of a TFCD in a homeotropic cell of CCN-47 at 29°C. Starting with (*a*) the voltage was held constant at 52.510 V for all frames. (*a*) $t = 0$ s; (*b*) $t = 25$ s; (*c*) $t = 50$ s; (*d*) $t = 95$ s; (*e*) $t = 100$ s.

region. Li and Lavrentovich [2] observed that the voltage at which nucleation occurs at different sites was different depending on the imperfections at the sites. Thus, the ramp rate of the voltage needs to be

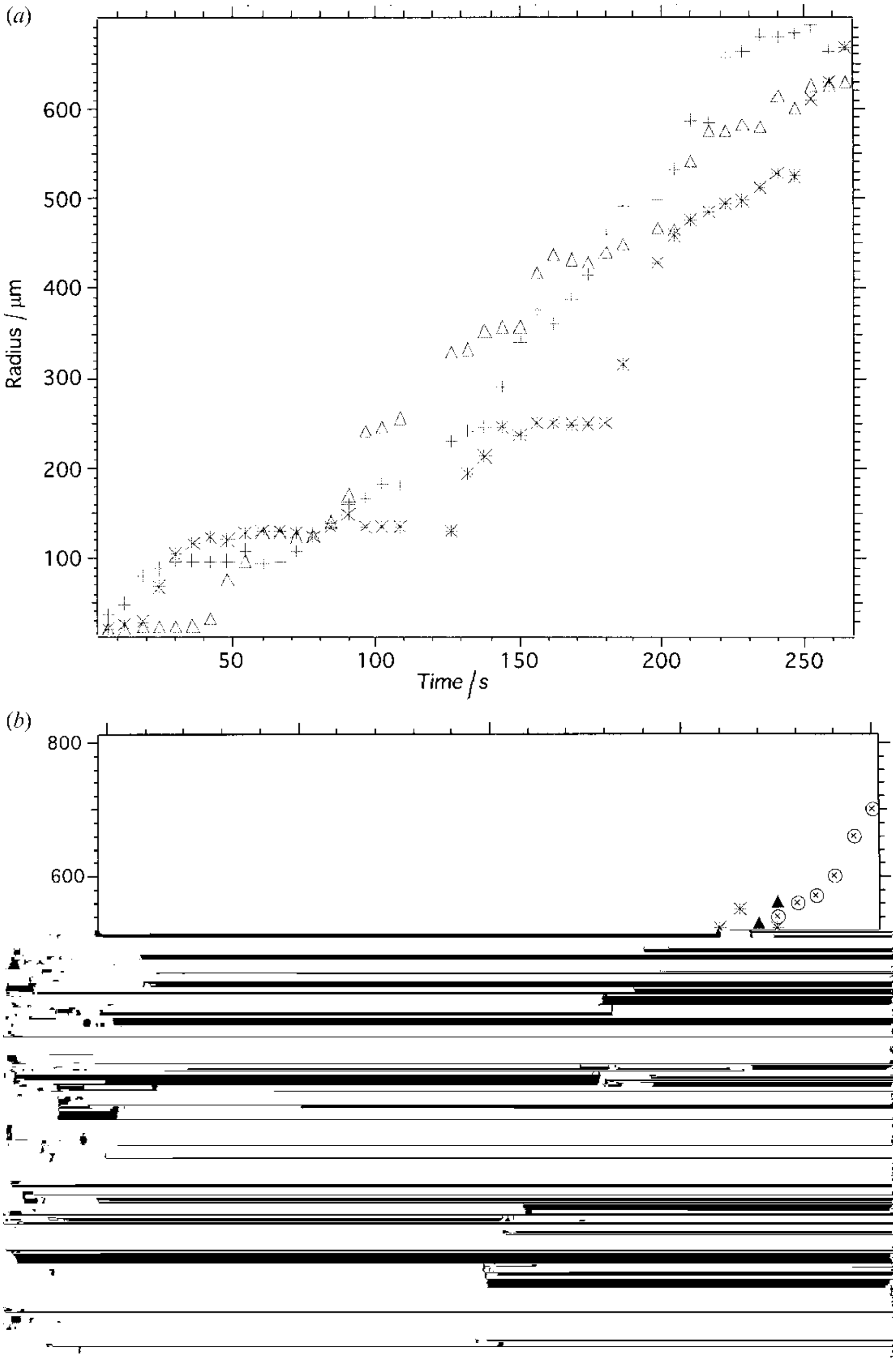

Figure 3. (*a*) Growth of stripe domain in pure CCN-47 at 22°C ($\Delta T = 7$°C). Symbols refer to measurements in three different directions from a horizontal line: + 145°; 225°; △ 320°. (*b*) Growth of TFCD and subsequently the stripe domain at 29°C ($\Delta T = 1$°C) in pure CCN-47. Symbols refer to three different measurements with respect to the horizontal: ▲ 45°, 135°; ⊗ 325°. Initial

experiments. The birefringence of CCN-47 is relatively low ($_{o} = 1.4723$, $_{e} = 1.5075$), which helps to maintain reasonable resolution of the imaging (about 1 µm).

The SmA cell was prepared in a manner similar to other experiments with kunipia particles; an electric field was used to create the TFCDs. In the FCPM, the

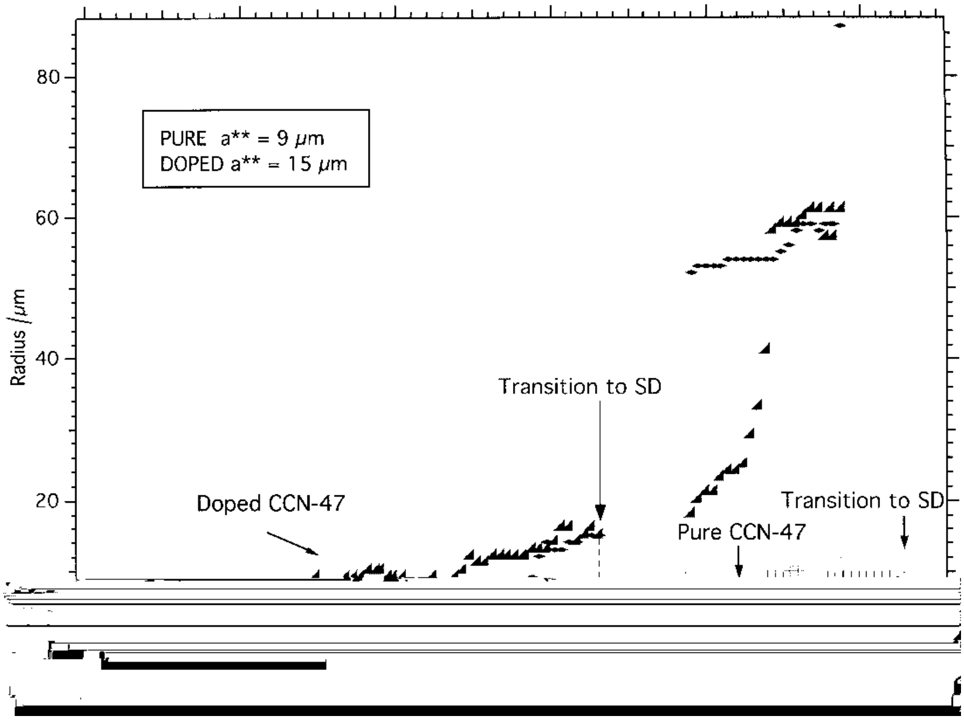

Figure 4. Determination of critical radius a^{**} in pure and doped CCN-47 at 22°C ($\Delta T = 7$°C for pure and 6°C for the doped).

laser beam scans the entire volume of the cell; the process takes a few seconds, or tens of seconds if the number of optical sections is large. Because of this limitation, we performed observations for the metastable TFCDs that remain in the cell after the electric field is switched off; their relaxation is slow and allows one to perform optical sectioning of the sample with sufficient resolution.

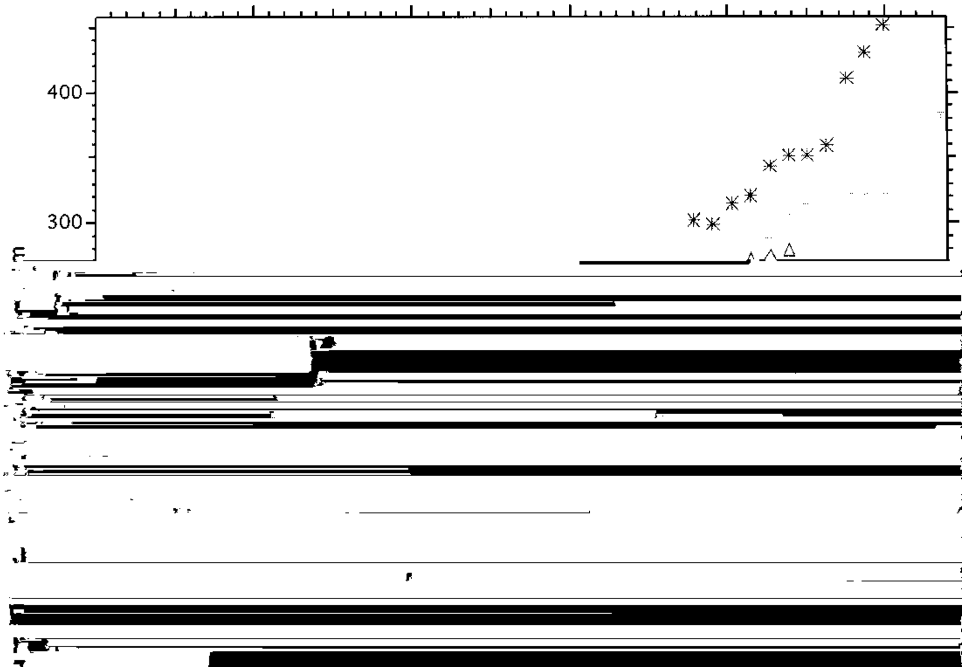

Figure 5. Growth of SD in doped CCN-47 at temperature 27°C ($\Delta T = 1$°C). Voltage held constant. Symbols refer to measurements in three different directions from a horizontal line: ✳ 38°, + 145°; △ 315°.

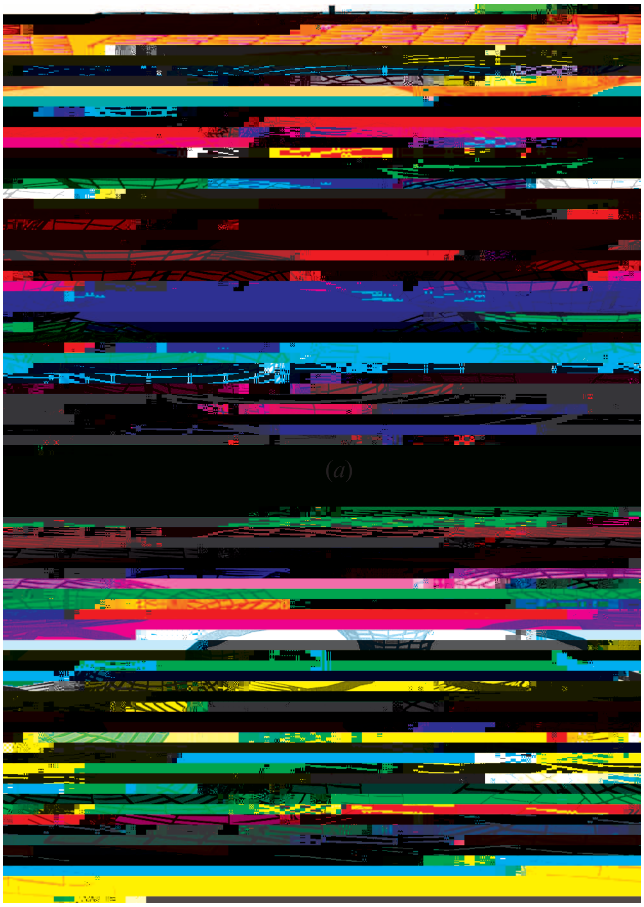
(*a*)

(*b*)

Figure 6. A TFCD in a smectic A liquid crystal nucleated (*a*) at the cell wall, (*b*) in the bulk of the cell.

Figure 7 shows the in-plane (*a*, *b*) and vertical (*c*) FCPM texture of the smectic cell with TFCDs. Since at the base of the TFCD the molecules are oriented horizontally, the base should be characterized by the maximum intensity of fluorescence. Figure 7 (*c*) clearly shows that the base of the TFCD is located in the bulk of the cell. This result is natural, as the homeotropic alignment at the bounding plates of the cell makes it difficult for the TFCD base to approach the boundaries.

5. Free energy considerations

5.1. *Nucleation of focal-conic domains*

The last result allows us to apply the model of bulk nucleation to the field-induced transition in the cells. According to [3], nucleation and growth of the TFCD from an ideal flat stack of layers is characterized by the free energy composed of elastic, dielectric and surface anchoring terms, all of which depend on the dimensionless order parameter $\rho = a/h$, where a is the radius of the domain and h is the thickness of the cell. Note that ρ gives a measure of the maximum layer tilt at the bounding surface with respect to the plates; this tilt θ changes from 0 at the periphery of the TFCD (where the layers become parallel to the plates) to its maximum value $\theta = \arctan(2a/h)$ at the points where the rotation symmetry axis of the TFCD crosses the bounding plates.

We use the following free energy functional for the sum f_b of bulk elastic and dielectric energy densities:

$$f_b = \frac{1}{2}K(\sigma_1+\sigma_2)^2 + \bar{K}\sigma_1\sigma_2 + \frac{1}{2}B\gamma^2 - \frac{1}{2}\varepsilon_0\,\varepsilon_a(\mathbf{E}\cdot\mathbf{n})^2 \qquad (1)$$

where σ_1 and σ_2 are the two principal local curvatures of the smectic layers, K is the splay elastic constant, K is the saddle–splay elastic constant, B is the compressibility modulus, ε_0 is the permittivity of free space, $\varepsilon_a = \varepsilon_{\|} - \varepsilon_{\perp} < 0$ is the dielectric anisotropy of SmA, $\varepsilon_{\|}$ and $\varepsilon_{\perp}$ are the relative electric permittivities (the subscripts refer to the director $\mathbf{n}$), $\mathbf{E}$ is the applied electric field and $\mathbf{n}$ is the director. The surface anchoring of lamellar phases is generally different from the anchoring of nematic liquid crystals, as not only the director, but also the layered structure, is strongly distorted near the bounding substrate [2]. For the nucleation problem, $\rho \ll 1$, the surface anchoring at the bounding plates can be neglected, as we have seen experimentally that the TFCDs nucleate in the bulk and do not disturb the layered structure near the bounding plates; however, it should be included in the discussion of the TFCD–SD transformation, as discussed later.

Using the model [3] developed for the magnetic field effect, and rewriting equation (17) in [3] in terms of the electric field (and neglecting the non-local field effects), one obtains the excess energy associated with the appearance of a TFCD (as compared with the energy of the uniform state under the action of the same electric field):

$$\begin{aligned}\Delta F = 2\pi K h\rho\Bigg[&\frac{\pi}{2}\ln 2 + L(\operatorname{arcctg} 2\rho)\\ &+ 2\operatorname{arcctg} 2\rho\left(\ln\frac{h\rho}{\xi} - 2\right)\\ &+ \operatorname{arctg} 2\rho\,\ln\frac{\rho h}{\xi(4\rho^2+1)^{\frac{1}{2}}} - \frac{1}{\rho}\ln\left(1+4\rho^2\right)\Bigg]\\ &- 2\pi\bar{K}h\left[\pi\rho - 2\rho\operatorname{arctg} 2\rho + \ln\left(1+4\rho^2\right)\right]\\ &+ \frac{\pi}{24}\varepsilon_a\varepsilon_0 E^2 h^3\left[8\rho^2 - 6\rho\operatorname{arctg} 2\rho\right.\\ &\left.+ \ln\left(1+4\rho^2\right) + 4\pi\rho^3 - 8\rho^3\operatorname{arctg} 2\rho\right] \qquad (2)\end{aligned}$$

y
x, P
P
Intensity Scale:

Figure 7. Fluorescence confocal polarizing microscopy texture of a field-induced focal-conic domain in the smectic A phase of CNN-47 doped with kunipia particles. Frames (*a*) and (*b*) represent horizontal (,) optical slices of thickness 1 μm taken from the middle plane of the cell that contains the base of the domain. Polarization of light is parallel to the -axis in (*a*) and to the -axis in (*b*). Line ''c'' shows the location of the vertical cross-section of the cell, depicted in frame (*c*). Frame (*c*) shows the vertical ( ) cross-section of the domain; lines ''a'' mark the location of frames (*a*) and (*b*). The maximum intensity of the fluorescent light is in the regions where $\hat{\mathbf{n}}\|\mathbf{P}$.

where ξ is the core radius of the circular defect and $L(\ )$ is Lobachevskiy's function

$$L(\ ) = -\int_0 \ln\cos\ \mathrm{d}$$

$$= \ln 2 - \frac{1}{2}\sum_{i=1}^{?}(-1)^{i-1}\frac{\sin 2i}{i^2}. \qquad (3)$$

Figures 8 (*a*) and 8 (*b*) show $\Delta F(\rho, E)$ as the function of the domain radius and the applied field, calculated using equations (2) and (3) with $h=36\,\mu\mathrm{m}$ $K=10^{-6}$ dyn, $\bar{K}=0$, $\varepsilon_a=-10$ [2]. Lobachevskiy's function is calculated with accuracy up to the first 40 terms in equation (3), using *Mathematica* Version 4.2.

The free energy (2) can be expanded for small $\rho \ll 1$:

$$\Delta F = A_1\rho + A_2\rho^2 + A_3\rho^3 + A_4\rho^4 + \ldots \qquad (4)$$

where the coefficients are

$$A_1 = 2\pi^2 Kh(\beta - 2 - \bar{K}/K). \qquad (5)$$

Here $\beta = \ln(2h\rho/\xi) \approx c$ (for $a \gg \xi$ the logarithmic dependence is weak);

$$A_2 = 4\pi Kh\left(\ln\sqrt{2} - \beta - 3\right) \qquad (6)$$

$$A_3 = \frac{\pi^2}{6}\varepsilon_0\varepsilon_a E^2 h^3. \qquad (7)$$

The linear coefficient A_1 is always positive (otherwise the SmA planar state would not be stable). We will assume $K = 0$. The third term A_3 is defined solely by the field contribution.

The dependences $\Delta F(\rho, E)$ for small ρ, figure 8 (*b*), clearly demonstrate the first order character of the transition. The function $\Delta F(\rho)$ goes through a maximum $\Delta F^* = \Delta F(\rho^*)$ at some critical radius ρ^* that defines the critical TFCD nuclei. Only the TFCDs of a sufficiently large radius $\rho > \rho^*$ transform the metastable uniform state into the stable defect state. The TFCDs with $\rho < \rho^*$ (embryos) are unstable and will decay.

The energy barrier that separates the two states is brought about by the [illegible] leading elastic term in the expansion (4). This term scales practically *linearly* with ρ and this explains why the barrier always exists and is located in the region of relatively small ρ: the driving force, in accordance with equation (7), contributes oJ/F07.5nTf-(nTjl.

feature is the result of Friedel's 'law of impenetrability' which states that two TFCDs cannot penetrate each other [8, 9]. In other words, the interaction of two TFCDs is of steric nature [1, 9].

The growth of $a > a^*$ to $a = a^{**}$ in the pure material at 29°C appears to be fairly linear, figure 3 (*b*). Moreover this growth occurs at constant voltage. This behaviour is reminiscent of the Avrami model of classical kinetic theory [10]. According to this model, in first order transformations nuclei of the product phase grow to reach a critical size, dependent on time and temperature. The physical properties of importance are: (i) nucleation rate per unit volume, which is a function of the activation energy for the molecular migration involved in the transformation and the critical free energy barrier, and (ii) the growth rate of the product phase, which depends on the undercooling at the growth interface [11]. The dynamics of the

coefficient in SmA strongly depends on the elastic constants, $W = \alpha(KB)^{\frac{1}{2}}$ in our model, one would expect W to decrease with temperature [2]. Therefore, ρ_s^{**} should depend on temperature and is likely to increase with temperature, which is consistent with our experimental data: a^{**} varies from about 10 μm at 22°C in figure 4 to 50–70 μm for the higher temperature of 29°C a TFCD is rather complex, the simple SD model explains it at least qualitatively. The main reason for the TFCD–SD transformation is the surface anchoring. In an expanding TFCD, the SmA layers make a progressively larger angle with the anchoring-imposed orientation, $\theta \to \pi/2$, as the TFCD radius increases. In an elongating SD, the nearly constant width ρ_s limits the maximum tilt of the SmA layers from the anchoring-imposed alignment, $\theta = \arctan \rho_s$, $\theta < \pi/2$. Therefore, elongation via SD is energetically preferable over the uniform expansion of TFCDs when the surface anchoring is non-zero, despite the fact that the elastic cost of the SD is high because the central SD plane is a plane defect of the tilt grain boundary defect type. The quantitative SD model demonstrates indeed that above some critical voltage U^{**}, there is a range of SD widths for which the SD line tension becomes negative, implying that these domains will grow by increasing their length. The range of the SD widths for which the energy is negative is rather broad for a20yJ/F11Tf9.05(n1787TD(U)Tj/F21Tf0.5007.8(TD(U)Tw/F151Tf1.00157TD(U)Tj/F21T

Copyright of Liquid Crystals is the property of Taylor & Francis Ltd and its content may